

Evolution of a quasi-two-dimensional shear layer in a soap film flow

Cite as: Phys. Fluids **32**, 124112 (2020); <https://doi.org/10.1063/5.0030319>

Submitted: 22 September 2020 • Accepted: 02 December 2020 • Published Online: 17 December 2020

Aparna Korlimarla and  Peter Vorobieff



[View Online](#)



[Export Citation](#)



[CrossMark](#)

ARTICLES YOU MAY BE INTERESTED IN

[On the similarities between the resonance behaviors of water balloons and water drops](#)
Physics of Fluids **32**, 124113 (2020); <https://doi.org/10.1063/5.0031388>

[Bubble entrapment during head-on binary collision with large deformation of unequal-sized tetradecane droplets](#)

Physics of Fluids **32**, 122114 (2020); <https://doi.org/10.1063/5.0029179>

[The law of the wall: A new perspective](#)

Physics of Fluids **32**, 121401 (2020); <https://doi.org/10.1063/5.0036387>

[LEARN MORE](#)

APL Machine Learning

Open, quality research for the networking communities

COMING SOON

Evolution of a quasi-two-dimensional shear layer in a soap film flow

Cite as: Phys. Fluids 32, 124112 (2020); doi: 10.1063/5.0030319

Submitted: 22 September 2020 • Accepted: 2 December 2020 •

Published Online: 17 December 2020



View Online



Export Citation



CrossMark

Aparna Korlimarla^{1,a)} and Peter Vorobieff^{2,b)}

AFFILIATIONS

¹ Adobe, 345 Park Avenue, San Jose, California 95110, USA

² University of New Mexico, Albuquerque, New Mexico 87131, USA

Note: This paper is part of the Special Topic, Interfaces and Mixing, and Beyond.

^{a)}Email: aparna.korlimarla@gmail.com

^{b)}Author to whom correspondence should be addressed: kalmoth@unm.edu

ABSTRACT

A quasi-two-dimensional shear layer is produced by merging two gravity-driven flows of soap film at different average velocities. The Kelvin–Helmholtz instability dominates the evolution of the shear layer, similar to what is observed in three-dimensional shear layers. However, the constraints that effectively limit the flow to two spatial dimensions have a considerable influence on the development of secondary instabilities and transition to turbulence. Nearly 40 cm downstream in the flow, two two-dimensional instabilities are observed, namely, vortex-pairing and secondary Kelvin–Helmholtz instability. The development of secondary instabilities and transition to turbulence in the flow is also affected by the interaction of the flowing soap film with boundary layers forming in the air surrounding the flowing soap film in the direction normal to the plane of the film. This becomes apparent when the flow is analyzed quantitatively in terms of the mixing interface length and fractal dimension. Initially, the mixing interface length grows exponentially with the downstream distance; however, beyond a certain distance, the growth stops. For the fractal dimension of the mixing interface in our quasi-two-dimensional shear layer, we have observed a peak value of 1.27 as compared to 1.34 reported in the literature for a corresponding section of a three-dimensional shear layer. For scales larger than ~ 1 cm, interaction with air begins to dominate as the leading mechanism of dissipation. Coupling with boundary layers in air near the soap film drains energy from the large flow features and apparently “freezes” its evolution, producing “fossil” turbulence at large downstream distances.

Published under license by AIP Publishing. <https://doi.org/10.1063/5.0030319>

I. INTRODUCTION

Shear flows are ubiquitous in nature and are present in a vast variety of applications. The classical instability characterizing a shear layer with an abrupt transition between two layers of fluid moving in parallel with disparate velocities is the Kelvin–Helmholtz (KH) instability,^{1,2} leading to the formation of a row of vortices of the same sign, which have a distinctive “cat’s eye” morphology³ if the flow is visualized with a tracer tagging one of the two fluid layers. The behavior of real shear flows transitioning to turbulence is more complex because instability amplitude growth soon becomes nonlinear, and a variety of secondary instabilities develop.⁴ In three-dimensional (3D) flows with nominally two-dimensional initial conditions, the secondary instabilities in a shear layer are also inherently

three-dimensional and lead to disordered flow that transitions to turbulence.

While unconstrained flows naturally default to three-dimensional turbulence, in some important cases, geometric or other constraints suppress fluid motion in one direction, leading (with some simplifications) to two-dimensional (2D) hydrodynamics that can be useful in the description of large-scale planetary phenomena (atmospheric, oceanic, and magnetospheric) in astrophysics and in plasma physics.^{5,6}

Here, it is worth noting that in 2D, turbulence itself is different: instead of an energy cascade from large (injection) scales to small (viscous dissipation) scales, there are two cascades: an inverse energy cascade from injection scale to larger scales and an enstrophy cascade from injection scale to small scales.⁵ The range of flow

instabilities possible in 2D is much narrower than in 3D, and KH instability plays a very prominent role in the transition to 2D turbulence.

While there are many numerical studies of 2D flows, a reasonably clean laboratory implementation of 2D hydrodynamics governed by Navier–Stokes equations and transitioning to turbulence is not very easy to achieve: a spatially constrained fluid flow is likely to be dominated by the boundary conditions in the directions of the constraint. In 1980, Kraichnan and Montgomery actually noted that “two-dimensional turbulence has the special distinction that it is nowhere realized in nature or the laboratory but only in computer simulations.”⁵ Since then, advances in experimental techniques led to the development of several laboratory arrangements for the studies of 2D hydrodynamics (and turbulence), including electromagnetically forced thin fluid layers (refer to Ref. 6 for a thorough review), magnetized electron columns,⁷ and soap films. The latter were originally proposed for 2D hydrodynamics studies as early as the 1920s by none other than Dewar.⁸ Practical use of soap films as an affordable and versatile 2D hydrodynamics testbed began in the 1980s⁹ and led to experimental confirmation^{10,11} of the Kraichnan–Batchelor theory of 2D turbulence.⁵ It must be noted that Kraichnan and Montgomery’s admonition still holds true, as all these experiments reproduce 2D Navier–Stokes hydrodynamics only within limits that must be taken into careful consideration.

Within these constraints, soap film flows continue to serve as a useful model for studies of quasi-2D hydrodynamic phenomena, with advances made in both the understanding of the film physical properties such as Marangoni elasticity¹² and surface tension¹³ and diagnostics. Among the latter are a recent adaptation of the Schlieren visualization technique for soap films¹⁴ and the development of the feature correlation velocimetry¹⁵ diagnostic, which relies on cross correlation analysis of short-wavelength variations on the film surface captured using a high-speed camera. While earlier studies of soap films focused on classical flows (cylinder wakes and grid turbulence), more recently, researchers’ attention expanded to flows around flapping filaments¹⁶ and wakes behind triangular objects.¹⁷ Another notable study showing the adaptability of the soap-film technique presents the results for soap-film flows past rotating hydrophobic and non-hydrophobic cylinders,¹⁸ with dramatic changes in the wake patterns attributable to both the rotation rate and cylinder surface hydrophobicity. However, the basics of the soap-film apparatus have not changed much, with many of the recent studies still using the gravity-driven inclined design originally developed in Los Alamos National Laboratory¹¹ and refined at the University of New Mexico.¹⁹

Taking into account the importance of the KH instability for 2D hydrodynamics and the versatility of soap films as a laboratory model of 2D flow, it would seem logical that a shear layer experiment would be implemented in soap films. Developing such an implementation proved challenging. Soap-film shear flow in cylindrical geometry has been used to conduct effective viscosity measurements of the soap film,²⁰ but this experiment reproduced a Couette flow, not a shear layer. One possibility to produce a shear layer-like pattern in flowing gravity-driven soap film is to insert a bent plate into the flow, constraining and accelerating one part of the film and expanding and slowing down the other part.²¹ This arrangement affects not only the flow velocity but also the film thickness, in a sense producing an analog of compressible flow at a non-trivial Mach number.

Here, we present a simple setup based on a well-known inclined soap-film tunnel, which makes it possible to study a shear layer in quasi-2D flow, leading to the development of the KH instability. Its evolution demonstrates some noteworthy features due to both the dimensionally constrained nature of the setup and the coupling between the soap-film flow and the surrounding air, as described below.

II. EXPERIMENTAL SETUP AND DATA ACQUISITION

The experimental arrangement is an evolution of the inclined soap-film channel.¹⁹ The channel is mounted on a modular frame with three independent segments, as shown in Fig. 1. These segments are two vertical supports on the sides and a 2.7 m beam stretched between them. The beam is attached to vertical rails on the centerline of each support. The angle of the beam with the horizontal can be varied from 0° to 30°. The mean elevation of the beam from the floor is also adjustable. We used an angle of 10° and a mean elevation of 60 cm in the experiments described here.

The three-segment frame supports the other components of the soap film channel. The modifications of the gravity driven soap film tunnel required to produce a shear layer flow are implemented at the top end of the tunnel. Unlike the simple inclined soap-film tunnel,¹⁹ our arrangement has two upper reservoirs. Each of them is comprised of a funnel with a coarse filter and a valve at the bottom to control the flow rate. They are mounted at different elevations and connected to a pair of nozzles, with the flows merging at the end of the expanding section, as illustrated in Fig. 1. Adjustment of the elevation of the reservoirs and the flow rate from each nozzle leads to a difference between the mean freestream velocities of the flows merging at the beginning of the parallel section. From the top reservoirs, the soap solution is driven by gravity through nozzles and between a pair of 0.78 mm diameter nylon wires (referred to as main wires). The flows from the two upper reservoirs merge between the upstream supports at the beginning of the parallel-flow section. At the downstream end of the channel, the wires are attached to a tensioner spring mounted on the center rail of the vertical support. At the upstream end, the wires are connected to elliptical cross section plastic nozzles. A plastic tube connects each nozzle to the bottom of the corresponding upper reservoir. The clamping position of the tube can be changed to vary the flow rate and the mean freestream velocity. To establish the flow, the main wires are pulled together, with a soap solution from both of the upper reservoirs running over them. Once the flow is established, the wires are stretched apart at the supports at the edges of the parallel-flow section, forming a gently inclined gravity-driven “conveyor belt” of soap solution supplied from the two top reservoirs and held flat by surface tension. The soap-film thickness in the apparatus is approximately 10 μm.¹⁹ The ratio of the dimensions of the film in the parallel-flow section (length:width:thickness) is thus about 135 000:12 000:1.

Submicrometer-sized titanium dioxide particles are used as tracers for flow visualization. In most of the experiments described here, the tracer was only put into one of the reservoirs at the top, facilitating visualization of the mixing interface.

Finally, the lower reservoir (a long open container) is mounted on the beam. In most soap-film channel setups, the soap solution can be removed from the lower reservoir and pumped back into the

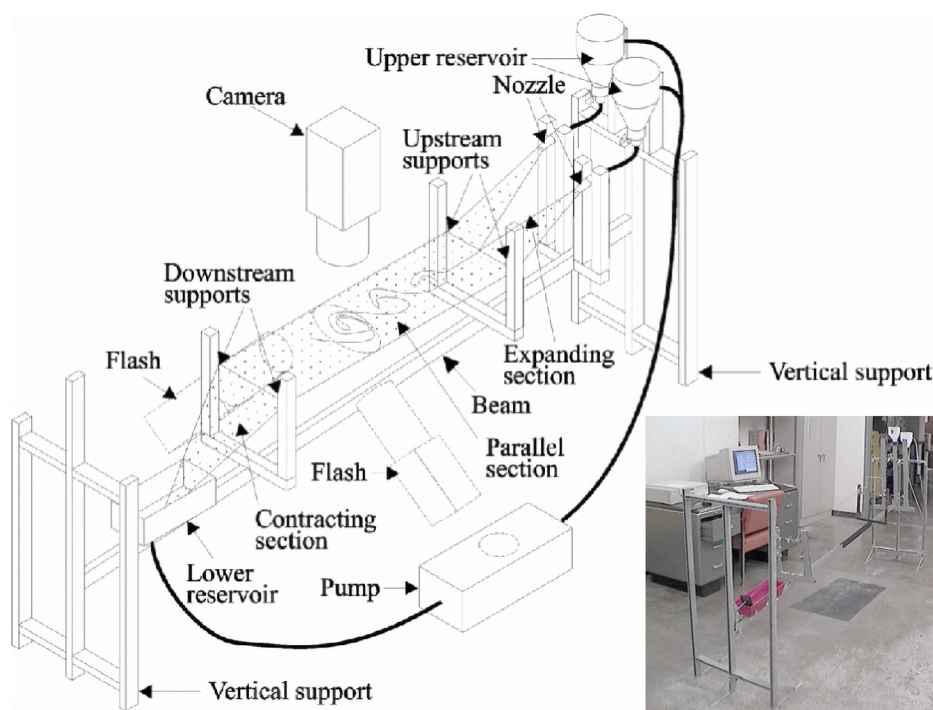


FIG. 1. Schematic of the experimental setup. Inset shows the actual view.

upper reservoir. In the experiments presented here, the recirculating flow was not established because only one of the reservoirs contained tracer.

The geometric parameters of the arrangement are as follows: The length of the expanding section (from the nozzle exhaust to the upstream pair of supports) is 0.66 m with slopes for the two reservoirs varying between 5° and 30°. The parallel section is 1.35 m, angled at 2.5°, and 0.12 m wide. The contracting section is ~0.33 m with a tilt of 30°.

After the construction of the apparatus described above, we observed liquid dripping at the point where the two flows from the upper reservoirs merged. This dripping disturbed the flow pattern, producing a noticeable fluctuation in the film thickness fed by accumulations of the solution at the merging point. We addressed this issue by adding a drain tube at the merging point of the two flows, as shown in Fig. 2(a). The difference produced by the drain tube is illustrated by Fig. 2(b). This plot shows velocity profiles acquired by particle image velocimetry (PIV, cross-stream distance on the

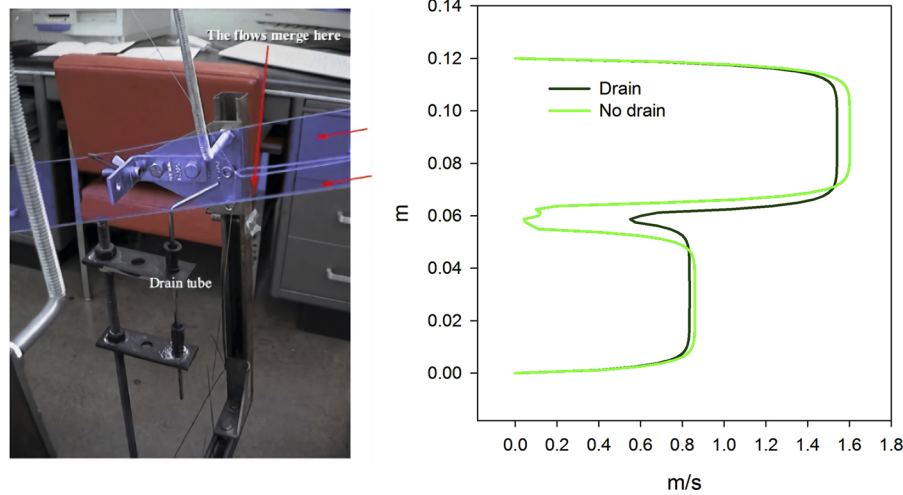


FIG. 2. Left: drain tube. Right: velocity profiles 2 cm downstream from the merging point with and without the drain tube. PIV diagnostics used to acquire velocity profiles are described in Refs. 19 and 22.

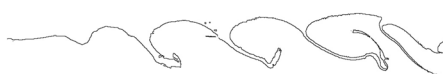


FIG. 3. Left: instantaneous image of the mixing interface. Right: traced interface contour.

y -axis and downstream velocity on the x -axis) 2 cm downstream from the merging point for a film of a lateral width of 12 cm. The PIV arrangement we used, its resolution, and interrogation uncertainties are described in detail elsewhere.^{19,22} For these experiments, we used a lower concentration of tracer ($\sim 10^{-6}$ by volume), with both reservoirs seeded. We confirmed that film 1 had a higher mean velocity than film 2. In the case of the system without the drain tube, a prominent velocity profile defect was observed at the merging point, with velocity dropping to zero due to the accumulation of the soap solution in the boundary layers of the wires joining together. In the case of the system with the drain tube, the velocity profile of the flow at the merging point shows a finite velocity (~ 0.5 m/s). The velocity profile defect at the merging point is also much narrower because the slow-moving fluid accumulating at the merging point is physically removed from the flow. For the experiments presented in this paper, the drain-tube arrangement was used.

The soap solution used in our experiments is 98% tap water and 2% commercial liquid soap. One liter of the soap solution in each reservoir is sufficient for running the soap film for several hours without adding any solution in the reservoirs. The film is illuminated by using xenon arc flash lamps, and the timing of the flashes is controlled by using a stream function generator. Images are acquired with a digital video camera (JVC GR 2000, 24 bits/pixel at a resolution of 1024×768 pixels), which is mounted on a heavy duty camera tripod. Images of the mixing interface are obtained at different downstream locations and analyzed. Titanium dioxide tracer particles that were put into one of the two reservoirs had a volume fraction of $6.0 \pm 0.5 \times 10^{-5}$. Figure 3 shows an example of the mixing-interface image. The darker region (film 2) of the film is the flow from the reservoir without the tracer, and the brighter (blue) region (film 1) is from the reservoir with the tracer.

We used public domain software GIMP²³ to trace the mixing interface. The tracing procedure was implemented as follows: First, a local equalization filter with a 256-pixel aperture was applied to the images to remove nonuniformities in lighting. Then, a histogram of the image was produced, and a mean brightness value is recorded. Finally, a brightness isocontour for this mean value was imaged. An example of the processed image is shown in right image in Fig. 3.

III. OBSERVATIONS

As the fast and slow films merge, they form a continuous flow with a growing interfacial perturbation, leading to the formation

of periodic vortex patterns at the interface shown in Fig. 4. This figure shows a mosaic of images of the shear flow with the downstream distance (in centimeters) marked from the merging point. We observe Kelvin–Helmholtz vortices at the interface, with a characteristic wavelength λ , defined as the distance between consecutive vortices, of ~ 1.9 cm, repeatable from experiment to experiment. The vortices driven by the primary instability start rolling up at a downstream distance of about 5 cm, while the secondary instabilities become apparent much farther downstream, with the downstream distance of the onset of each instability varying from experiment to experiment.

Figure 5 shows images of the secondary instabilities we observe. In the left image of Fig. 5, we see small-scale vortices advected by the large-scale vortex structures. These vortices are likely a manifestation of the secondary shear-driven instability (secondary Kelvin–Helmholtz vortices).

In the right image of Fig. 5, we see large-scale vortices pairing up (the vortex-pairing instability). It is noteworthy that the two instabilities correspond to two inertial ranges that may exist in 2D turbulent flow—the enstrophy cascade range directed from large scales toward smaller scales (secondary Kelvin–Helmholtz vortices are smaller than the primary vortices driving them) and the inverse energy cascade directed toward larger scales. The latter would correspond to the coarsening of the flow structure due to vortex pairing. The onsets of the two secondary instabilities do not appear

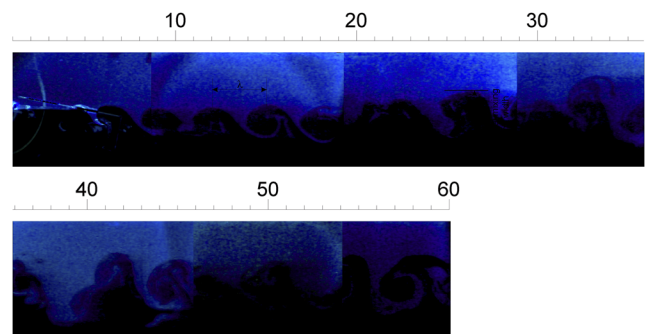


FIG. 4. Mosaic of images of the shear flow. Ruler shows the distance (in cm) from the merging point. The image also shows references to the instability wavelength λ and peak-to-trough extent of the mixing interface.

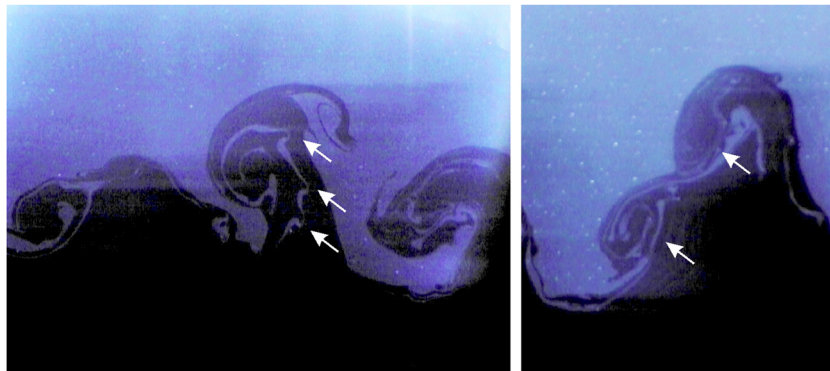


FIG. 5. Left: secondary Kelvin–Helmholtz vortices. Right: apparent vortex pairing. Arrows point to features of interest. Best images from a sequence are shown.

correlated, with the secondary Kelvin–Helmholtz vortices first appearing at 25 ± 5 cm downstream and the vortex pairings happening at 30 ± 5 cm downstream.

In the results presented below, we quantitatively analyzed images acquired at 13 downstream locations, with 50% overlap at the downstream distance 0 cm–35 cm from the merge point and with no overlap further downstream. The data extraction at each location used instantaneous images separated by times on the order of seconds—sufficient for the images to be statistically independent (with average velocity 50 cm/s, it takes for the flow less than 0.2 s to advect any flow structures out of the field of view of the camera).

IV. ANALYSIS AND DISCUSSION

The KH instability amplifies all the perturbation wavelengths, so the presence of a specific scale in the flow is likely to manifest itself in the periodicity of the KH vortex structures, sometimes in a non-trivial fashion.²⁴ In the case of KH instabilities in the vicinity of boundary layers, it was reported²⁵ that $\lambda \sim 10\delta$, where δ is the boundary layer thickness. We observe $\lambda \sim 19$ mm, whereas the boundary layers at the supporting wires are characterized by $\delta \sim 2$ mm (Fig. 3), consistent with these observations.

An important feature of our quasi-2D observations is that the interface between the seeded and unseeded fluid remains well-defined throughout the entire range of downstream distances we imaged. This is quite different from 3D shear layers, where a mixing transition²⁶ rapidly leads to greatly enhanced mixing and blurs the interface. In fact, the mixing transition was originally discovered in 3D mixing layers.²⁷

As described in Sec. III, the mixing of the two layers commences at low downstream distances, with the width of the mixing zone increasing with the downstream distance. Figure 6 plots the mixing interface width (averaged for the 7.3 cm field of view) as the function of the downstream distance. This figure also shows a mosaic image of the shear flow as reference. Each data point is based on multiple crest-to-trough mixing-zone width measurements extracted from six instantaneous images. This plot clearly shows that the variation falls in two regions. In the first region, where the downstream distance is less than 30 cm, the mixing interface length increases nearly linearly with the downstream distance. Classical theories describe²⁸ linear growth rates for early KHI development. The linear KHI growth also manifests in compressible fluids with

and without magnetohydrodynamic effects²⁹ and in moving mixing layers with a continuous velocity profile.³⁰ The latter case is particularly important in the context of the present study. Later in its evolution, KHI enters a nonlinear growth regime with saturation³¹ and with secondary instabilities appearing.

In the second region, where the downstream distance is greater than 30 cm, the growth of the mixing interface width slows down (here, it is helpful to remember that the downstream distance increases with time for flow features moving with the film), reaching a constant value slightly above 3 cm. The slowdown and cessation of the interfacial perturbation growth cannot be attributed solely to geometric constraints, as the moving film is appreciably wider (12 cm) than this saturation value. Secondary instabilities described in Sec. III may play a role in the growth saturation, but it is more likely caused by scale-dependent coupling between the soap-film flow and the boundary layers forming in the surrounding air, described by Chomaz³² and later experimentally characterized using almost the same setup as here (with two reservoirs being the

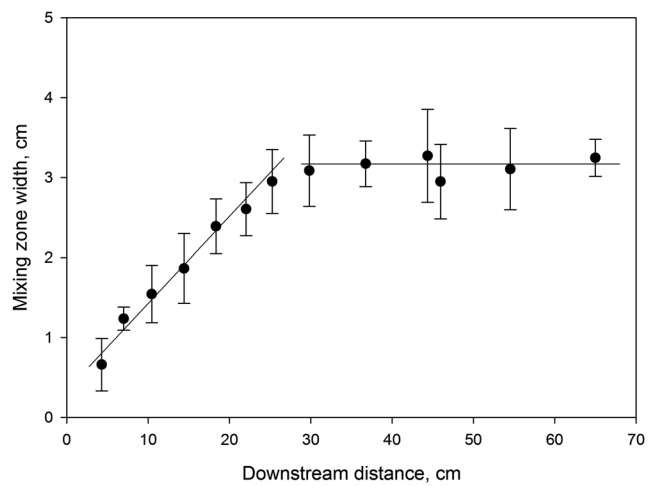


FIG. 6. Mixing zone width (vertical extent in the images) vs downstream distance x with a linear fit for $x < 30$ cm and a constant-value fit after that. The linear fit shown in the plot has a coefficient of determination $r^2 = 0.97$ for $x < 30$ cm. For $x > 30$ cm, the mixing zone width is constant (3.14 cm with 95% confidence).

only substantial difference).^{19,22} This coupling becomes prominent for structures on scales ~ 1 cm and larger (consistent with the vortex scales we observe 30 cm and further downstream), and it effectively “sucks” the energy of the mixing-layer vortices at large downstream distances. Accordingly, we observe previously formed flow features being advected downstream, but not evolving further.

Next, let us consider the mixing interface length. It is an important property because of its influence on mixing in the flow. One of the phenomenological features of transition to turbulence is the greatly enhanced mixing.³³ On the microscale, mixing is diffusive, and its enhancement is due to the interface stretching and folding in the flow.^{34,35} Mixing interface length, usually measured in a planar cross section of the flow, offers a convenient quantitative characteristic of such interface stretching,^{36–38} highly relevant for understanding mixing dynamics in shear flows.³⁹

Studies of mixing-interface length in soap films, however, have not been conducted, despite the obvious advantage of their constrained geometry for this diagnostic. We extracted the mixing lengths from the black-and-white mixing interface contour images (refer to Fig. 3) as follows: The dimensionless length of the contour was assessed as the number of pixels comprising the contour, normalized by the horizontal pixel resolution of the image, and scaled by the horizontal physical image extent. Thus, for a perfectly unperturbed interface, the interface length should be unity times 7.3 cm. Figure 7 plots the mixing interface length (with the horizontal image extent factored out) as it increases with the downstream distance up to $x \sim 30$ cm and then retains a nearly constant value farther downstream. We also show a curve fit to the data in the 0 cm–30 cm downstream range and in the initial 30 cm of the downstream distance using an exponential fit $L = 2.16e^{0.057x}$, where x is the downstream distance in cm, with a corresponding coefficient of determination $r^2 = 0.99$. Further downstream, the value remains effectively constant (12 at 95% confidence). Exponential growth of the mixing interface length is a notable feature of chaotic mixing in three dimensions,^{40,41} as well as in flows geometrically constrained

in one dimension.³⁷ The cessation of this exponential trend at downstream distances beyond 30 cm is consistent with our earlier-stated notion of “frozen” flow features advected downstream without evolving.

One more important quantifiable feature of a mixing interface is its fractal dimension. The fractal properties of turbulent flows⁴² have been studied extensively, with a particularly relevant result predicted theoretically and obtained experimentally for a jet flow.⁴³ For the outer boundary of a turbulent jet discharged into a quiescent fluid, the fractal dimension theoretically predicted for a two-dimensional (2D) outer surface of the jet is 2.33 (suggesting 1.33 for a planar section of the same surface). The experiment (using flow visualization with fluorescent material to tag the jet) produces 2.35 ± 0.05 for the same surface.⁴³ For a box-counting estimate of the fractal dimension⁴⁴ of planar sections of a turbulent jet, similar results were also reported by Flohr and Olivari.⁴⁵

We applied an implementation of the box-counting technique originally developed for tracking an interface in a planar section of mixing flow⁴⁶ to the soap-film mixing interface data, producing the results in Fig. 8. Over the first 30 cm of the shear layer, the interfacial fractal dimension increases nonlinearly. Further downstream, it retains a constant value around 1.27. Note that the same box-counting algorithm implementation applied to three-dimensional shear layer data produces a terminal value around 1.34.⁴⁷ What could account for the difference? One possible explanation could be that the soap-film mixing layer is geometrically confined to two dimensions and cannot develop three-dimensional turbulence with mixing transition. However, the scalings usually associated with fractal features of fully developed 2D turbulence are $4/3$ and $7/4$,⁴⁸ at least not lower than the predictions for three dimensions. Accordingly, the more likely reason for the terminal value we observe is interaction with the surrounding air that slows down the evolution of the flow features.

The far-downstream behavior of the soap-film flow may be similar to what is known as fossil turbulence.^{49,50} flow features that

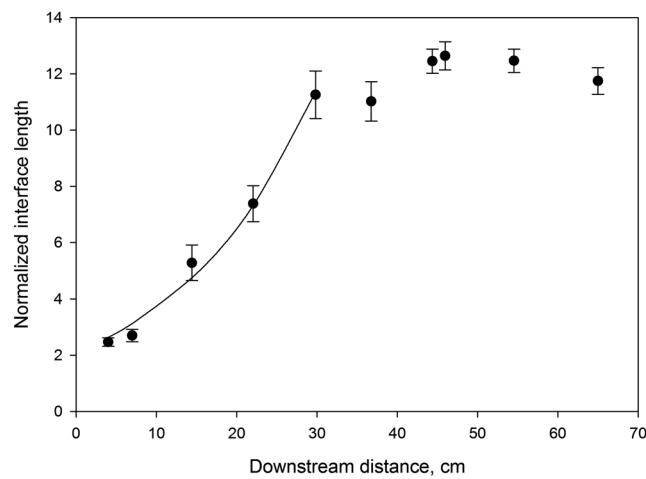


FIG. 7. Mixing interface length vs downstream distance. Exponential fit also shown for the first 30 cm. Further downstream, the interface length remains effectively constant (12.0 at 95% confidence).

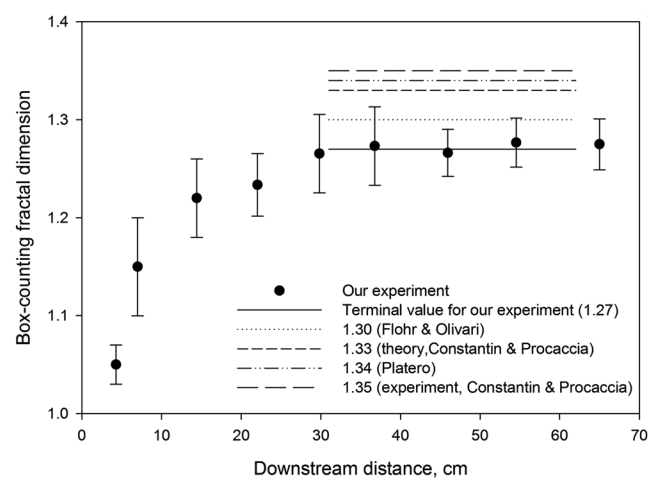


FIG. 8. Box-counting fractal dimension (assessed over 7.3 cm windows) of the mixing interface as the function of the downstream distance. Values reported in the literature^{43,45,47} are also shown.

persist in the flow that is no longer turbulent are the remnants of earlier turbulence.

V. SUMMARY

We describe the construction of a quasi-two-dimensional shear-layer generator based on a well-characterized inclined, gravity-driven soap-tunnel design. The generator provides a simple but useful testbed for investigations of shear-driven instabilities in a dimensionally constrained geometry. One of the fluids is seeded with submicrometer-sized titanium dioxide particles to facilitate visualization of the mixing interface and quantification of its features at different downstream distances.

The fundamental features of the Kelvin–Helmholtz instability observed in this experimental apparatus are very similar to 3D realizations. The instability manifests perturbation amplitude growth that follows a linear trend and produces a roll-up of vortices with a distinctive “cat’s eye” morphology. However, later-time evolution of the flow is characterized by the development of secondary instabilities known in 3D (secondary Kelvin–Helmholtz roll-ups), features peculiar to 2D hydrodynamics in general (vortex merging), and features unique to soap-film flows (coupling of larger structures in the film with surrounding air flow, resulting in “fossilization” of the 2D shear layer turbulence). Mixing transition, a key characteristic of 3D shear layers, is also notably absent from the 2D shear layer.

Future work could include comparison with 2D numerical modeling results to further elucidate the role of air drag and, possibly, advancement of the diagnostics to facilitate simultaneous particle-tracer tracking (which would require seeding both mixing streams with tracers at a low uniform density) and interface tracking (with fluorescent dye injected into one stream only).

ACKNOWLEDGMENTS

This research was supported by American Chemical Society Petroleum Research Fund (Grant No. 40218-AC9).

DATA AVAILABILITY

The data that support the findings of this study are available from the corresponding author upon reasonable request.

REFERENCES

- ¹W. Thomson, “XLVI. Hydrokinetic solutions and observations,” *London, Edinburgh Dublin Philos. Mag. J. Sci.* **42**(281), 362–377 (1871).
- ²H. Helmholtz, “XLIII. On discontinuous movements of fluids,” *London, Edinburgh Dublin Philos. Mag. J. Sci.* **36**(244), 337–346 (1868).
- ³R. S. Scorer, “Billow mechanics,” *Radio Sci.* **4**(12), 1299–1308 (1969).
- ⁴B. J. Bayly, S. A. Orszag, and T. Herbert, “Instability mechanisms in shear-flow transition,” *Annu. Rev. Fluid Mech.* **20**(1), 359–391 (1988).
- ⁵R. H. Kraichnan and D. Montgomery, “Two-dimensional turbulence,” *Rep. Prog. Phys.* **43**(5), 547 (1980).
- ⁶G. Boffetta and R. E. Ecke, “Two-dimensional turbulence,” *Annu. Rev. Fluid Mech.* **44**, 427–451 (2012).
- ⁷K. S. Fine, A. C. Cass, W. G. Flynn, and C. F. Driscoll, “Relaxation of 2D turbulence to vortex crystals,” *Phys. Rev. Lett.* **75**, 3277–3280 (1995).
- ⁸J. Dewar, “Soap films as detectors: Stream lines and sound,” *Proc. R. Inst.* **24**, 197–259 (1923).
- ⁹Y. Couder, “Two-dimensional grid turbulence in a thin liquid film,” *J. Phys. Lett.* **45**(8), 353–360 (1984).
- ¹⁰B. K. Martin, X. L. Wu, W. I. Goldburg, and M. A. Rutgers, “Spectra of decaying turbulence in a soap film,” *Phys. Rev. Lett.* **80**(18), 3964 (1998).
- ¹¹M. Rivera, P. Vorobieff, and R. E. Ecke, “Turbulence in flowing soap films: Velocity, vorticity, and thickness fields,” *Phys. Rev. Lett.* **81**(7), 1417 (1998).
- ¹²I. Kim and S. Mandre, “Marangoni elasticity of flowing soap films,” *Phys. Rev. Fluids* **2**(8), 082001 (2017).
- ¹³A. Sane, S. Mandre, and I. Kim, “Surface tension of flowing soap films,” *J. Fluid Mech.* **841**, R2 (2018).
- ¹⁴M. I. Auilal, F. C. Hebrero, R. Sosa, and G. Artana, “Schlieren technique in soap film flows,” *Exp. Fluids* **58**(5), 38 (2017).
- ¹⁵K. Siddharth, M. V. Panchagnula, and T. John Tharakan, “Feature correlation velocimetry for measuring instantaneous liquid sheet velocity,” *J. Fluids Eng.* **139**(9), 091401 (2017).
- ¹⁶S. Feng, C. Chen, Q. Huang, and T. Zhou, “Experimental study on the flapping dynamics for a single flexible filament in a vertical soap film,” *J. Fluid Struct.* **86**, 236–246 (2019).
- ¹⁷I. Kim, “Separated rows structure of vortex streets behind triangular objects,” *J. Fluid Mech.* **862**, 216–226 (2019).
- ¹⁸N. G. Chikkam and S. Kumar, “Flow past a rotating hydrophobic/nonhydrophobic circular cylinder in a flowing soap film,” *Phys. Rev. Fluids* **4**(11), 114802 (2019).
- ¹⁹D. Georgiev and P. Vorobieff, “The slowest soap-film tunnel in the Southwest,” *Rev. Sci. Instrum.* **73**(3), 1177–1184 (2002).
- ²⁰B. Martin and X. L. Wu, “Shear flow in a two-dimensional Couette cell: A technique for measuring the viscosity of free-standing liquid films,” *Rev. Sci. Instrum.* **66**(12), 5603–5608 (1995).
- ²¹P. Vorobieff and R. E. Ecke, “Fluid instabilities and wakes in a soap-film tunnel,” *Am. J. Phys.* **67**(5), 394–399 (1999).
- ²²T. Shakeel and P. Vorobieff, “Decaying turbulence in soap films: Energy and enstrophy evolution,” *Exp. Fluids* **43**(1), 125–133 (2007).
- ²³O. S. Kylander and K. Kylander, *GIMP: The Official Handbook With CDROM* (Coriolis Value, 1999).
- ²⁴D. Olmstead, P. Wayne, J.-H. Yoo, S. Kumar, C. R. Truman, and P. Vorobieff, “Experimental study of shock-accelerated inclined heavy gas cylinder,” *Exp. Fluids* **58**(6), 71 (2017).
- ²⁵A. D. M. Walker, “The Kelvin–Helmholtz instability in the low-latitude boundary layer,” *Planet. Space Sci.* **29**(10), 1119–1133 (1981).
- ²⁶P. E. Dimotakis, “The mixing transition in turbulent flows,” *J. Fluid Mech.* **409**, 69–98 (2000).
- ²⁷J. H. Konrad, “An experimental investigation of mixing in two-dimensional turbulent shear flows with applications to diffusion-limited chemical reactions,” Ph.D. thesis, California Institute of Technology, 1977.
- ²⁸S. Chandrasekhar, *Hydrodynamic and Hydromagnetic Stability* (Courier Corporation, 2013).
- ²⁹A. Suzuki, H. R. Takahashi, and T. Kudoh, “Linear growth of the Kelvin–Helmholtz instability with an adiabatic cosmic-ray gas,” *Astrophys. J.* **787**(2), 169 (2014).
- ³⁰R. Chong, O. Lafitte, and J. Cahen, “Linear growth rate for Kelvin–Helmholtz instability appearing in a moving mixing layer,” *Phys. Scr.* **2008**(T132), 014039.
- ³¹R. Keppens, G. Tóth, R. H. J. Westermann, and J. P. Goedbloed, “Growth and saturation of the Kelvin–Helmholtz instability with parallel and antiparallel magnetic fields,” *J. Plasma Phys.* **61**, 1–19 (1999).
- ³²J.-M. Chomaz, “The dynamics of a viscous soap film with soluble surfactant,” *J. Fluid Mech.* **442**, 387–409 (2001).
- ³³M. Lesieur, *Turbulence (Edition 2013)* (EDP Sciences, 2014).
- ³⁴J. Ottino, *The Kinematics of Mixing: Stretching, Chaos, and Transport* (Cambridge University Press, 1989), Vol. 3.
- ³⁵J. Krasnodebski, M. O’Sullivan, D. Tew, E. Greitzer, F. Marble, C. Tan, and T. Tillman, “Enhanced mixing with streamwise vorticity,” *Prog. Aerosp. Sci.* **33**, 323 (1997).

- ³⁶C. J. Bourdon and J. C. Dutton, "Shear layer flapping and interface convolution in a separated supersonic flow," *AIAA J.* **38**(10), 1907–1915 (2000).
- ³⁷R. Truesdell, P. Vorobieff, L. Sklar, and A. Mammoli, "Mixing of a continuous flow of two fluids due to unsteady flow," *Phys. Rev. E* **67**(6), 066304 (2003).
- ³⁸P. Vorobieff, C. R. Truman, A. M. Ragheb, G. S. Elliott, J. K. Laystrom-Woodard, D. M. King, D. L. Carroll, and W. C. Solomon, "Mixing enhancement in a multi-stream injection nozzle," *Exp. Fluids* **51**(3), 711–722 (2011).
- ³⁹A. Bandopadhyay, P. Davy, and T. Le Borgne, "Shear flows accelerate mixing dynamics in hyporheic zones and hillslopes," *Geophys. Res. Lett.* **45**(21), 11–659, <https://doi.org/10.1029/2018gl079914> (2018).
- ⁴⁰F. Schönenfeld, V. Hessel, and C. Hofmann, "An optimised split-and-recombine micro-mixer with uniform 'chaotic' mixing," *Lab Chip* **4**(1), 65–69 (2004).
- ⁴¹J. R. Pacheco, "Mixing enhancement in electro-osmotic flows via modulation of electric fields," *Phys. Fluids* **20**(9), 093603 (2008).
- ⁴²K. R. Sreenivasan and C. Meneveau, "The fractal facets of turbulence," *J. Fluid Mech.* **173**, 357–386 (1986).
- ⁴³P. Constantin, I. Procaccia, and K. R. Sreenivasan, "Fractal geometry of isoscalar surfaces in turbulence: Theory and experiments," *Phys. Rev. Lett.* **67**(13), 1739 (1991).
- ⁴⁴J. Theiler, "Estimating fractal dimension," *J. Opt. Soc. Am. A* **7**(6), 1055–1073 (1990).
- ⁴⁵P. Flohr and D. Olivari, "Fractal and multifractal characteristics of a scalar dispersed in a turbulent jet," *Physica D* **76**(1-3), 278–290 (1994).
- ⁴⁶P. Vorobieff, P. M. Rightley, and R. F. Benjamin, "Shock-driven gas curtain: Fractal dimension evolution in transition to turbulence," *Physica D* **133**(1-4), 469–476 (1999).
- ⁴⁷C. Platero, "Fractal dimension evolution in a shear layer instability," Master's thesis, University of New Mexico, 2003.
- ⁴⁸D. Bernard, G. Boffetta, A. Celani, and G. Falkovich, "Conformal invariance in two-dimensional turbulence," *Nat. Phys.* **2**(2), 124–128 (2006).
- ⁴⁹J. D. Woods, V. Högström, P. Misme, H. Ottersten, and O. M. Phillips, "Fossil turbulence," *Radio Sci.* **4**(12), 1365–1367 (1969).
- ⁵⁰C. H. Gibson, "Internal waves, fossil turbulence, and composite ocean microstructure spectra," *J. Fluid Mech.* **168**, 89–117 (1986).